393, 54 (1998); N. Thouveny et al., Nature 371, 503 (1994); E. C. Grimm et al., Science 261, 198 (1993); H. Mommersteeg, thesis, University of Amsterdam (1998).
4. J. Johnsen, W. Dansgaard, J. W. C. White, Tellus Ser. B 41, 452 (1989).
5. K. M. Cuffey et al., J. Glaciol. 40, 341 (1994); K. M. Cuffey et al., Science 270, 455 (1995).
6. S. Johnsen, D. Dahl-Jensen, W. Dansgaard, N. Gundestrup, Tellus Ser. B 47, 624 (1995).
7. J. Schwander et al., J. Geophys. Res. 102, 19483 (1997).
8. J. P. Severinghaus et al., Nature 391, 141 (1998).
9. A. Mariotti, Nature 303, 685 (1983).
10. H. Craig, Y. Horibe, T. Sowers, Science 242, 1675 (1988).
11. J. Schwander, in The Environmental Record in Glaciers and Ice Sheets, H. Oeschger and C. C. Langway Jr., Eds. (Wiley, New York, 1989), pp. 53–67.
12. S. Chapman and T. G. Cowling, The Mathematical Theory of Non-Uniform Gases (Cambridge Univ. Press, Cambridge, 1970).
13. M. Leuenberger, C. Lang, J. Schwander, J. Geophys. Res. 104, 22163 (1999).
14. V. Boersma-Klein and A. E. De Vries, Physica 32, 717 (1966).
15. We determined $\delta^{15}N$ on gas from samples of the GRIP ice core from depths between 2552 and 2567 m [69,215 to 71,925 years B.P. ice age (17), about 68,850 to 71,100 years mean gas age (7)]. Seventy-four samples (each about 21 g) from 36 different depth levels were analyzed. The mean resolution for the samples is thus 40 cm or ~75 years ice age (~60 years mean gas age difference). The resolution is higher during the transition to the DO 19, namely ~25 cm (64 years ice age and 15 years mean gas age difference; the gas resolution due to gas mixing by diffusion and close-off process is lower, namely 50 to 100 years). The air was released from the ice with a melt extraction technique. After evacuation, the ice samples underwent a melting-refreezing cycle twice to liberate the enclosed gas from bubbles and clathrates. The gas then passed through a water trap cooled with liquid nitrogen and was frozen at 20 K. After this procedure, less than 0.005% of the gas was left. The samples were then analyzed with a MAT-250 mass spectrometer for several isotope and element ratios. ^{15}N and ^{14}N were measured simultaneously in relation to a standard gas with a reproducibility of 0.02 per mil. Results are given as $\delta^{15}N$, that is, the per mil deviation from the atmospheric isotope ratio, $^{15}N/^{14}N$. The overall uncertainty is less than 0.05 per mil. $\delta^{18}O_{ice}$ measured with the standard CO_2 equilibrium method in Copenhagen and Reykjavik (17) shows an uncertainty of 0.05 per mil.
16. H. R. Phillpot and J. W. Zillman, J. Geophys. Res. 75, 4161 (1970).
17. S. Johnsen et al., J. Geophys. Res. 102, 26397 (1997).
18. M. A. Hutterli, R. Röthlisberger, R. C. Bales, Geophys. Res. Lett. 26, 1691 (1999); J. Schwander et al., J. Geophys. Res. 98, 2831 (1993); C. M. Trudinger et al., J. Geophys. Res. 102, 6747 (1997).
19. P. A. Mayewski et al., J. Geophys. Res. 102, 26345 (1997).
20. W. R. Kapsner et al., Nature 373, 52 (1995).
21. D. Dahl-Jensen, S. J. Johnsen, C. U. Hammer, H. B. Clausen, J. Jouzel, in Ice in the Climate System, NATO ASI Series, vol. 112 (Springer-Verlag, Berlin, 1993), pp. 517–532; J. Jouzel et al., Quat. Res. 31, 135 (1989).
22. C. Charles, Nature 385, 681 (1997).
23. E. J. Brook, T. Sowers, J. Orchardo, Science 273, 1087 (1996).
24. Because the atmospheric methane is believed to have been primarily related to the tropical and subtropical hydrological cycle [A. Dällenbach et al., in preparation; J. Chappellaz et al., Nature 366, 443 (1993)], a small methane variation at DO 19 [as indicated by the methane record (23), but in low resolution] could mean small temperature and precipitation changes in these regions.
25. J. Jouzel et al., J. Geophys. Res. 102, 26471 (1997).
26. This work is a contribution to the Greenland Ice Core Project (GRIP), a European Science Foundation program with eight nations and the European Economic Commission collaborating to drill through the central part of the Greenland Ice Sheet. This special study was financially supported by the Bundesamt für Energie and the Swiss National Science Foundation (including the Swiss Priority Programme Environment) as well as the European Community project MILECLIM (contract ENV4-CT97-0659). We thank T. Stocker for helpful discussion and comments and P. Nyfeler for technical assistance.

19 May 1999; accepted 7 September 1999

Seismic Consequences of Warm Versus Cool Subduction Metamorphism: Examples from Southwest and Northeast Japan

Simon M. Peacock[1]* and Kelin Wang[2]

Warm and cool subduction zones exhibit differences in seismicity, seismic structure, and arc magmatism, which reflect differences in metamorphic reactions occurring in subducting oceanic crust. In southwest Japan, arc volcanism is sparse and intraslab earthquakes extend to 65 kilometers depth; in northeast Japan, arc volcanism is more common and intraslab earthquakes reach 200 kilometers depth. Thermal-petrologic models predict that oceanic crust subducting beneath southwest Japan is 300° to 500°C warmer than beneath northeast Japan, resulting in shallower eclogite transformation and slab dehydration reactions, and possible slab melting.

During subduction, variably hydrated basalts and gabbros of the oceanic crust transform to eclogite, a relatively dense rock consisting primarily of garnet and omphacite (Na-Ca clinopyroxene). The transformation of hydrated metabasalt to eclogite releases substantial amounts of H_2O (*1*) and increases the density of subducting slabs (*2*). Kirby *et al.* (*3*) proposed that dehydration reactions trigger intermediate-depth (50 to 300 km) intraslab earthquakes and suggested that deeper intraslab earthquakes observed in cold subduction zones may reflect kinetic hindrance of eclogite formation. In a given subduction zone, the depth and nature of eclogite formation and slab dehydration reactions depends on the pressure (P)–temperature (T) conditions encountered by the subducting oceanic crust. Temperatures at depth in subduction zones vary because of variations in convergence rate, thermal structure (age and sediment thickness) of the incoming lithosphere, and possibly rates of shear heating (*4*). We present thermal models for the subduction zones of southwest (SW) and northeast (NE) Japan and examine the metamorphic evolution of subducting oceanic crust.

In many subduction zones, detailed seismic investigations reveal the presence of a thin (<10 km thick), low seismic-velocity layer coinciding with the zone of thrust and intermediate-depth earthquakes (*3, 5, 6*). The seismic velocity of eclogite is comparable to mantle peridotite, thus the dipping low seismic-velocity layer is generally interpreted as subducted oceanic crust that has not transformed to eclogite (*3*). Beneath SW Japan, subducted oceanic crust of the Philippine Sea plate is marked by a layer with low P-wave (V_P = 6.6 to 6.9 km s^{-1}) and S-wave (V_S = 3.8 to 3.9 km s^{-1}) velocity which extends to 60 km depth (*7*). Beneath NE Japan, the low-velocity layer, representing subducted oceanic crust of the Pacific plate, persists to 150 km depth and has slightly higher V_P ~ 7.5 km s^{-1} (*5, 8*). Beneath SW Japan, the maximum depth of intraslab earthquakes is ~50 to 65 km (*9*). In NE Japan, intraslab earthquake activity peaks at 125 km depth and extends to 200 km depth (*3*), and deep earthquakes occur down to 670 km depth (*5*).

Abundant Holocene volcanism occurs in NE Japan (Fig. 1) with a well-defined volcanic front located ~100 km above the top of the subducting Pacific plate (*5*). Most NE Japan arc lavas exhibit calc-alkaline geochemistry, which reflects partial melting in the mantle wedge triggered by the infiltration of aqueous fluids derived from the subducting slab (*10*). In SW Japan, Holocene volcanism is relatively sparse. Andesite and dacite erupted at Daisen and Sambe volcanoes in SW Japan (Fig. 1) are geochemically similar to adakites (*11*), which are interpreted to represent partial melts of subducted oceanic crust (*12*).

To understand subduction-zone processes operating at 50 to 200 km depth, we constructed two-dimensional, finite-element heat-transfer models for NE and SW Japan along the profiles

[1]Department of Geology, Arizona State University, Tempe, AZ 85287–1404, USA. [2]Pacific Geoscience Centre, Geological Survey of Canada, Sidney, BC V8L 4B2, Canada.

*To whom correspondence should be addressed. E-mail: peacock@asu.edu

depicted in Fig. 1 (*13*). The geometry of the subducting plates was constrained by seismic reflection studies (*14*) and Wadati-Benioff zone seismicity (*5, 15*). Existing surface heat flux data were used to estimate the rate of shear heating (Q_{sh}) along the subduction thrust; Q_{sh} = 0 W m^{-2} for SW Japan and 0.029 W m^{-2} for NE Japan down to 70 km depth. Sediment thickness at the trench is 1.4 km for SW Japan and 0.35 km for NE Japan (*15*). For NE Japan, we calculated the steady-state thermal structure for 130-million-year-old (Ma) oceanic lithosphere subducting at 91 mm year^{-1} (Fig. 2A). For SW Japan, the subduction of the fossil Shikoku Ridge beginning at 15 Ma (*16*) requires transient heat-transfer solutions (*17*). For SW Japan, we present the thermal structure resulting from subduction at a rate of 45 mm year^{-1} for 15 million years, during which the age of the incoming plate increases from 0 to 15 Ma (Fig. 2B). For the initial temperature condition, we used the steady-state solution for a 100-Ma slab subducting at 45 mm year^{-1}. On the basis of sensitivity tests using different parameters, we estimate uncertainties in the calculated thermal structure of subducted oceanic crust to be ±50 to 100°C, primarily due to uncertainties in the mantle-wedge flow model and thermal properties.

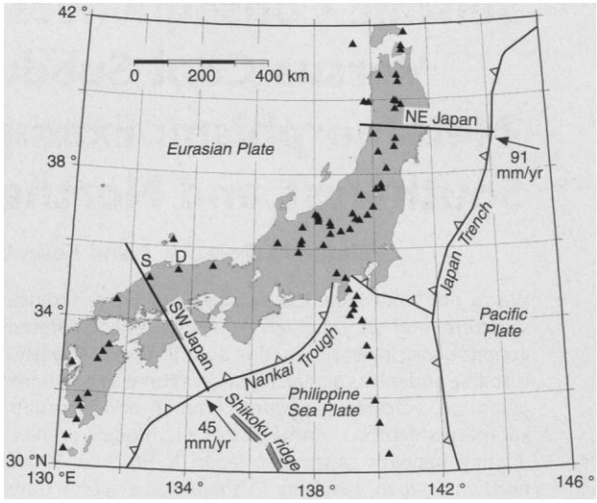

Fig. 1. Tectonic map of Japan showing Holocene volcanoes (solid triangles) (*20*), trenches (lines marked with open triangles), and location of thermal profiles. D, Daisen volcano; S, Sambe volcano.

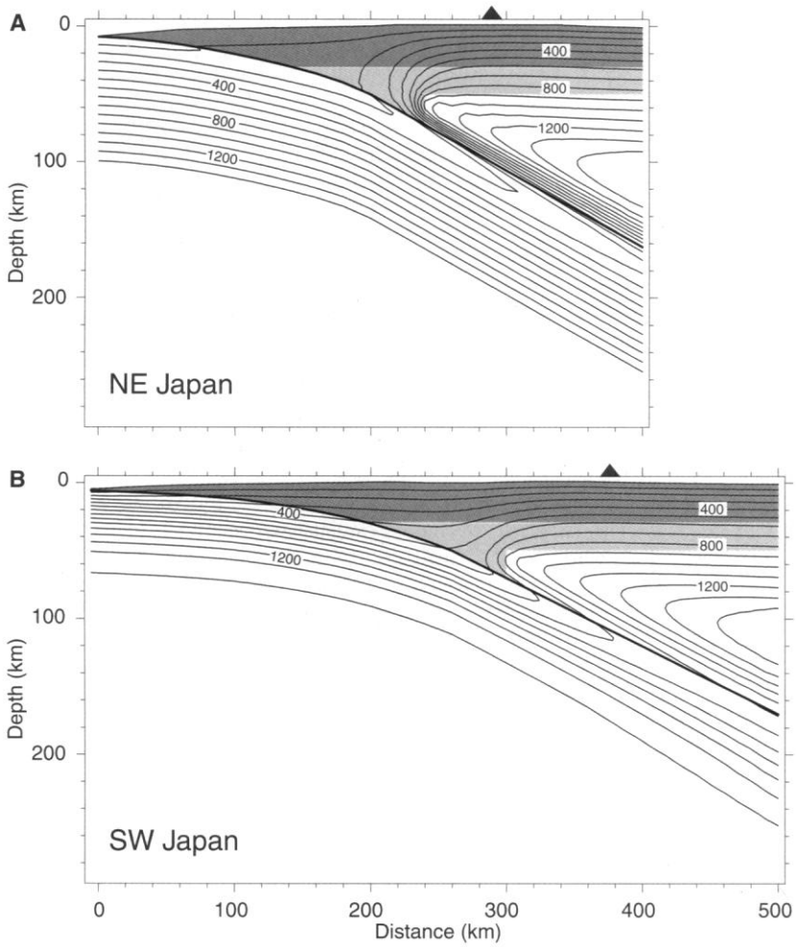

Fig. 2. Calculated thermal structure for (**A**) NE and (**B**) SW Japan subduction zones. Rigid Japan lithosphere is shaded with darker shading representing crust. Black triangles mark location of volcanic front. Contour interval = 100°C.

The subducting Pacific plate beneath NE Japan is cooler than the subducting Philippine Sea plate beneath SW Japan (Fig. 2). At 50 km depth, the calculated temperature along the slab/mantle interface is only 200°C for NE Japan, compared to 500°C for SW Japan. Beneath the volcanic front, the slab/mantle interface temperature is 500°C in NE Japan, compared to >800°C in SW Japan. In both subduction zones, maximum mantle-wedge temperatures beneath the volcanic front are ~1200°C.

To predict the sequence of metamorphic reactions within the subducting oceanic crust, we combined calculated *P-T* paths with a petrogenetic grid for metabasalts (Fig. 3). The eclogite metamorphic facies is bounded by the blueschist facies at low temperatures and by the amphibolite and granulite facies at high temperatures (Fig. 3A). The temperature-dependent blueschist → eclogite transition involves garnet-forming dehydration reactions, which release up to 5 weight % H_2O (*1*). In contrast, the amphibolite/granulite → eclogite transition involves the pressure-dependent anhydrous reaction of plagioclase to form omphacite + quartz. At T < ~900°C, hydrous minerals, including lawsonite, chlorite, amphibole, zoisite, and chlorotoid, are stable in the eclogite facies even though the primary minerals that define the eclogite facies, garnet and omphacite, are anhydrous (Fig. 3A) (*18, 19*). Thus, subducting oceanic crust that transforms to eclogite has the capacity to transport H_2O to greater depths. Partial melting in basaltic compositions is possible at temperatures as low as 650°C (Fig. 3A).

Pacific oceanic crust subducting beneath NE Japan passes through the lawsonite-blueschist facies (Fig. 3B). The top of the crust intersects the eclogite facies at ~110 km depth, whereas the base of the crust may not intersect the eclogite facies until depths >160 km, beyond the limits of our model (Fig. 3B). In contrast, Philippine Sea oceanic crust subducting beneath SW Japan passes through the

greenschist and epidote–blueschist/amphibolite facies and enters the eclogite facies at ~50 km depth. The different depths of predicted eclogite formation agrees well with the observed depth extent of the low seismic-velocity layer beneath NE Japan (150 km) and SW Japan (60 km). Furthermore, the lower V_P and V_S of the layer beneath SW Japan compared to NE Japan is consistent with the lower seismic velocities of greenschist and epidote–blueschist/amphibolite facies compared to the lawsonite-blueschist facies (*6*). In both subduction zones, the low seismic-velocity layer persists to depths where the subducting hydrous oceanic crust is predicted to transform to eclogite, suggesting that kinetic retardation of eclogite-forming reactions (*3*) may not be required.

Hydrous phases in the subducting oceanic crust remain stable to >160 km depth beneath NE Japan but only to 90 km beneath SW Japan. These depths are similar to the observed maximum depth of intraslab earthquakes in the two subduction zones and support the dehydration embrittlement model for intraslab earthquakes (*3*). The lack of intraslab earthquakes at depths >65 km beneath SW Japan may be a consequence of aseismic ductile behavior at $T > 600°C$. Beneath NE Japan, the peak in intraslab earthquake activity at 125 km depth may reflect fluids released by garnet-forming dehydration reactions in the upper part of the subducting crust (Fig. 3B). Intermediate-depth earthquakes beneath NE Japan define a double seismic zone (*5*); earthquakes in the lower seismic zone may be caused by dehydration reactions in subducting oceanic mantle.

Oceanic crust subducting beneath NE Japan is relatively cool and does not undergo partial melting (Fig. 3B). The abundant arc volcanism in NE Japan reflects partial melting in the overlying mantle wedge, presumably triggered by infiltration of aqueous fluids derived from the subducting slab. The calculated *P-T* paths for NE Japan suggest abundant H_2O may be subducted to >100 km depth, where dehydration reactions such as the garnet-forming reaction can release fluids beneath the hot core of the overlying mantle wedge. In contrast, the oceanic crust subducting beneath SW Japan is relatively warm, and calculated *P-T* paths approach the fluid-absent partial melting reaction associated with the breakdown of hornblende (Fig. 3B). Adakite-like lavas in SW Japan may reflect partial melting of the subducting slab (*11*). Beneath SW Japan, most of the water in the subducting oceanic crust is driven off at shallow depth (<50 km) and is not available to trigger partial melting of the mantle wedge, consistent with the relatively sparse volcanism and lack of normal calc-alkaline magmatism (*3*).

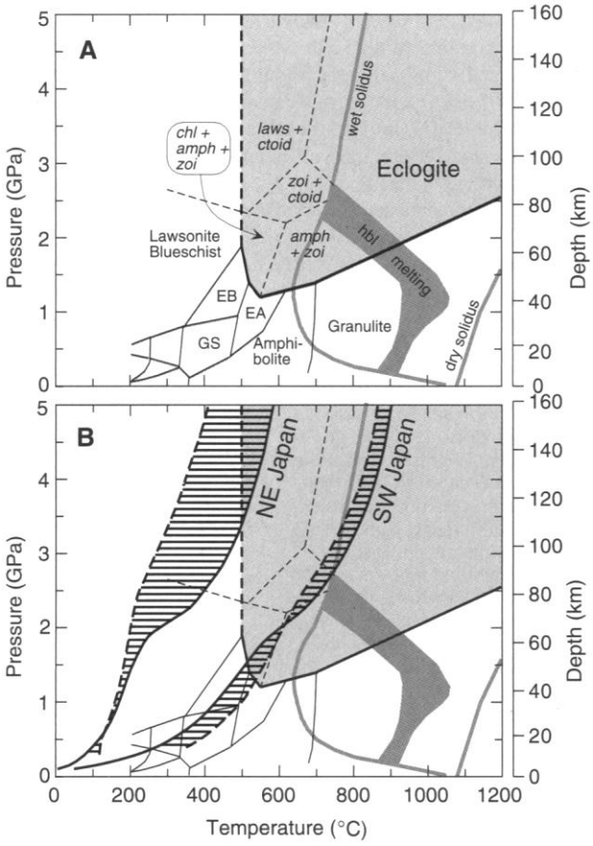

Fig. 3. Metamorphic conditions in oceanic crust subducted beneath NE and SW Japan. (**A**) Metamorphic facies (*21*), hydrous minerals (italics) stable in the eclogite facies (light gray) (*19*), and partial melting reactions (dark gray) for basaltic compositions (*21*). Thermodynamic calculations (*22*) suggest the blueschist → eclogite transition (dark dashed line) is nearly isothermal (~500°C), but this has not been experimentally confirmed. EA, epidote amphibolite; EB, epidote blueschist; GS, greenschist; amph, amphibole; chl, chlorite; ctoid, chlorotoid; laws, lawsonite; zoi, zoisite. (**B**) Calculated *P-T* conditions (horizontal lined area) for oceanic crust subducting beneath NE and SW Japan. Solid line, top of subducting oceanic crust; dashed line, base of subducting oceanic crust.

References and Notes

1. S. M. Peacock, *Geol. Soc. Am. Bull.* **105**, 684 (1993).
2. T. J. Ahrens and G. Schubert, *Rev. Geophys. Space Phys.* **13**, 383 (1975).
3. S. H. Kirby, E. R. Engdahl, R. Denlinger, in *Subduction: Top to Bottom*, G. E. Bebout *et al.*, Eds. (American Geophysical Union, Washington, DC, 1996), pp. 195–214.
4. S. M. Peacock, in (*3*), pp. 119–133.
5. A. Hasegawa, S. Horiuchi, N. Umino, *J. Geophys. Res.* **99**, 22295 (1994).
6. G. Helffrich, in (*3*), pp. 215–222.
7. See, for example, Y. Fukao, S. Hori, M. Ukawa, *Nature* **303**, 413 (1983); S. Hori, *Tectonophysics* **176**, 355 (1990).
8. T. Matsuzawa *et al.*, *Geophys. J. R. Astron. Soc.* **86**, 767 (1986).
9. M. Nakamura *et al.*, *Ann. Disaster Prev. Res. Inst. Kyoto Univ.* **40B-1**, 1 (1997).
10. See, for example, J. Gill, *Orogenic Andesites and Plate Tectonics* (Springer-Verlag, New York, 1981).
11. P. Morris, *Geology* **23**, 395 (1995).
12. M. J. Defant and M. S. Drummond, *Nature* **347**, 662 (1990).
13. The NE Japan and SW Japan grids consist of 720 and 936 eight-node isoparametric elements, respectively. In both models, radioactive decay produces 1.3 $\mu W\ m^{-3}$ in the upper crust (0 to 15 km depth) and 0.27 $\mu W\ m^{-3}$ in the lower crust (15 to 30 km depth). The thermal conductivities of the crust and mantle are 2.5 and 3.1 $W\ m^{-1}\ K^{-1}$, respectively. For the arc-side boundary condition, a continental geotherm was defined to yield a surface heat flux of 65 $mW\ m^{-2}$; the temperature at 95 km depth is 1450°C and increases at an adiabatic gradient of 0.3°C km^{-1} for depths >95 km. Where material is advecting through the arc-side boundary, we set the horizontal conductive heat flux to 0. For the trench-side boundary, we used oceanic geotherms [C. A. Stein and S. Stein, *Nature* **359**, 123 (1992)] of 130 Ma for NE Japan and 0 to 15 Ma for SW Japan with the seafloor and lower boundary kept at 0° and 1450°C, respectively. The thickness of the rigid lithosphere of Japan was fixed at 50 km, corresponding to the 850°C isotherm. In the mantle wedge, beneath the rigid lithosphere, flow induced by the subducting slab was approximated using an analytical corner flow solution [G. K. Batchelor, *An Introduction to Fluid Dynamics* (Cambridge Univ. Press, Cambridge, 1967)]. As depicted in Fig. 2, no flow was permitted in the tip of the mantle wedge in order to satisfy the surface heat flux data in NE Japan and to be consistent with dynamical subduction models [C. Kincaid and I. S. Sacks, *J. Geophys. Res.* **102**, 12295 (1997)]. Our model does not include magma generation and transport and therefore does not generate high temperatures beneath active volcanoes.
14. J. Ashi and A. Taira, in *Thermal Evolution of the Tertiary Shimanto Belt, Southwest Japan*, M. B. Underwood, Ed. (Geological Society of America, Boulder, CO, 1993), pp. 137–149; K. Suyehiro and A. Nishizawa, *J. Geophys. Res.* **99**, 22331 (1994).
15. K. Hirahara, *Tectonophysics* **79**, 1 (1981); D. Zhao, T. Matsuzawa, A. Hasegawa, *Phys. Earth Planet. Inter.* **102**, 89 (1997).
16. J. P. Hibbard and D. E. Karig, *Tectonics* **9**, 207 (1990).
17. K. Wang, R. D. Hyndman, M. Yamano, *Tectonophysics* **248**, 53 (1995).
18. D. A. Carswell, Ed., *Eclogite Facies Rocks* (Chapman & Hall, New York, 1990).
19. S. Poli and M. W. Schmidt, *J. Geophys. Res.* **100**, 22299 (1995).
20. T. Simkin and L. Siebert, *Volcanoes of the World* (Geoscience Press, Tucson, AZ, 1994).
21. C. W. Oh and J. G. Liou, *Island Arc* **7**, 36 (1998); see references in S. M. Peacock, T. Rushmer, A. B. Thompson, *Earth Planet. Sci. Lett.* **121**, 227 (1994).
22. B. W. Evans, *Lithos* **25**, 3 (1990).

23. Supported by NSF grants EAR 97-25406 and 98-09602 to S.M.P. Geological Survey of Canada contribution number 1999150.

14 June 1999; accepted 21 September 1999